J. Cent. South Univ. (2019) 26: 1687−1695
DOI: https://doi.org/10.1007/s11771-019-4125-4

Springer

Probabilistic seismic stability of three-dimensional slopes by pseudo-dynamic approach

PAN Qiu-jing(潘秋景)[1], QU Xing-ru(屈兴儒)[1], WANG Xiang(王翔)[1, 2]

1. Department of Civil Engineering, Central South University, Changsha 410075, China;
2. Department of Civil and Environmental Engineering, Hong Kong University of Science and Technology, Clear Water Bay, Kowloon, Hong Kong, China

© Central South University Press and Springer-Verlag GmbH Germany, part of Springer Nature 2019

Abstract: Probabilistic analysis is a rational approach for engineering design because it provides more insight than traditional deterministic analysis. Probabilistic evaluation on seismic stability of three dimensional (3D) slopes is studied in this paper. The slope safety factor is computed by combining the kinematic approach of limit analysis using a three-dimensional rotational failure mechanism with the pseudo-dynamic approach. The variability of input parameters, including six pseudo-dynamic parameters and two soil shear strength parameters, are taken into account by means of Monte-Carlo Simulations (MCS) method. The influences of pseudo-dynamic input variables on the computed failure probabilities are investigated and discussed. It is shown that the obtained failure probabilities increase with the pseudo-dynamic input variables and the pseudo-dynamic approach gives more conservative failure probability estimates compared with the pseudo-static approach.

Key words: seismic slope stability; pseudo-dynamic analysis; probabilistic analysis; Monte-Carlo simulation; failure probability; three-dimensional slop

Cite this article as: PAN Qiu-jing, QU Xing-ru, WANG Xiang. Probabilistic seismic stability of three-dimensional slopes by pseudo-dynamic approach [J]. Journal of Central South University, 2019, 26(7): 1687−1695. DOI: https://doi.org/10.1007/s11771-019-4125-4.

1 Introduction

Three-dimensional (3D) slope stability is a classical problem in geotechnical engineering, which has attracted many attentions among researchers and engineers. Generally, approaches adopted for evaluating slope stability can be sorted into limit equilibrium analyses [1−3], numerical simulations by means of finite element or finite difference methods [4, 5], and limit analysis methods [6−10]. Limit equilibrium methods consider global force and moment equilibriums inside a sliding body bounded by a presumed slip surface (linear, circular or logspiral) along which the soils meet the yield condition, e.g., the Mohr-Coulomb strength criterion for frictional soils. However, some prior assumptions with regard to inter-slice forces and sliding surface shapes are often required. The critical safety factor is obtained by optimization with respect to the slip surface pattern (or location). In limit equilibrium methods, none of solid mechanics equations is met inside or outside of the slip surface and no conceptions of plastic flow rule and kinematical admissibility are involved, thus the limit equilibrium solutions are neither upper-bound nor lower-upper estimations. Numerical simulation methods, without complementary assumptions required, can offer detailed information (stresses and deformations) on

Received date: 2019-01-14; **Accepted date:** 2019-03-22
Corresponding author: WANG Xiang; Tel: +852-69931903; E-mail: wang.irving.xiang@gmail.com; ORCID: 0000-0003-4972-8329

the slope behavior under external loadings. A main defect of numerical simulations is that they are usually time-consuming, and their solutions are often for a particular problem, practically intractable for parametric analysis. The kinematic approach of limit analysis, based on the theory of plasticity, is able to find an upper-bound estimate of collapse conditions by means of a work balance equation, for which the external work rate and the internal energy dissipations are both computed with respect to a pre-assumed kinematically admissible failure mechanism. An effective failure mechanism should obey kinematical boundary conditions and the flow rule associated with soil yield conditions.

In the past several decades, the kinematic approach of limit analysis has been widely employed to analyze slope stability in terms of critical heights or safety factors, and several kinematically admissible three-dimensional (3D) failure mechanisms were proposed, for instance the multi-blocks translational mechanism [6], the horn failure mechanism [7]. The classical horn failure mechanism inspired numerous subsequent investigations, based on the extensions of the horn failure mechanism to account for the destabilizing effects of seepage forces or pore-water pressures [8, 11−13], seismic loadings [14−18].

However, in previous studies [14−18], the pseudo-static approach is employed to consider the seismic effects which are treated as uniform inertial forces under constant accelerations. Although the procedures of pseudo-static approach are straightforward and relatively easy to be implemented, it fails to represent the dynamic nature of earthquakes, for example shaking durations and frequency, the amplification of accelerations and phase shifts because of finite shear wave propagations, and cannot offer a reliable assessment of seismic performance. In order to rectify this drawback, the pseudo-dynamic approach was proposed by STEEDMAN et al [19] to model the seismic response of earthquakes in terms of its duration, periodicity, phase change and amplification. The pseudo-dynamic approach has been adopted to evaluate seismic stability of retaining walls [20] and slopes with or without geosynthetics [9, 21, 22]. A contribution of this paper is to apply the pseudo-dynamic approach to slope stability using the 3D horn failure mechanism.

There are two sources of uncertainties in seismic slope stability; the first one is the variability of soil properties, e.g., soil friction angles and cohesions, and the second comes from seismic shakings, such as shear wave velocities and seismic coefficients. In order to account for uncertainties, these input parameters are often treated as random variables following specific distributions. In practice, probabilistic analysis is adopted to examine the safety degree (e.g., reliability index or failure probability) of structures subjected to random variability of input parameters. The topic of probabilistic slope stability has gained great attention in recent decades [23−26]. The second contribution in this work is to incorporate probabilistic concepts into the pseudo-dynamic kinematic slope stability using the method of Monte Carlo Simulation (MCS).

This work aims to implement probabilistic assessment of seismic stability of a slope by combining the kinematic approach of limit analysis with the pseudo-dynamic approach. The remaining of this paper is organized as follows. The second section introduces deterministic safety factor calculations of a 3D slope based on the upper-bound limit analysis and the pseudo-dynamic approach. Then the method of MCS is briefly presented with respect to computing failure probabilities. It is followed by probabilistic analysis in order to discuss the influences of pseudo-dynamic input parameters on the computed failure probabilities. This paper ends up with a conclusion.

2 3D slope stability by pseudo-dynamic approach

2.1 Horn failure mechanism

The 3D horn failure mechanism was firstly proposed by MICHALOWSKI et al [17] for slope stability in the context of the kinematical approach of limit analysis. Figure 1 shows a 3D slope with a height of H, width of B and inclination of β. The 3D horn failure mechanism is composed of two components, a curvilinear cone and a plane-strain insert. A cylindrical rotational velocity field is assumed in this mechanism, rotating around a horizontal axis passing point O with an angular velocity ω. The velocity of a point in the mechanism is equal to the product of the angular velocity and its distance to the rotating center.

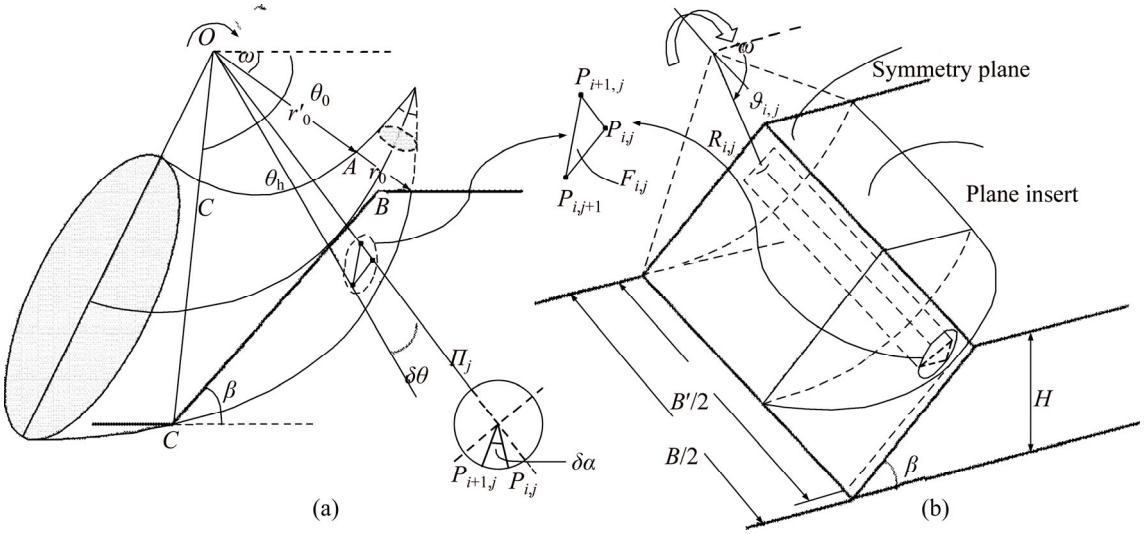

Figure 1 3D Horn failure mechanism of a slope: (a) 2D view; (b) 3D view

In the longitudinal symmetry plane, the curvilinear cone section (see Figure 1(a)) is bounded by two logarithmic spirals, which respects the normality rule that requires velocities to incline an angle φ with the failure surface (φ represents friction angle of Mohr-Coulomb medium). The cross-section of each radial plane, Π_j, is described by a circle whose radius can be determined by the two logarithmic spirals. The kinematic admissibility of this curvilinear cone section is validated and discretized by PAN et al [18]. The discretization involves to two angular parameters, $\delta\theta$ and $\delta\alpha$, by which the curvilinear cone surfaces are represented by a series of points, e.g., $P_{i,j}$, $P_{i,j+1}$, $P_{i,j+1}$. The discretization makes it possible to consider non-homogeneity of soil properties and seismic wave phase changes, avoiding complex integration computations.

In order to permit a transition to plane-strain situation when no limitation is applied to the slope width, the curvilinear cone body is artificially split into two halves between which a plane-strain insert is added. The geometry of the plane-strain insert is logarithmic spiral and it connects two curvilinear cone surfaces, which consist of the end parts of the failure mechanism (see Figure 1(b)).

2.2 Pseudo-dynamic approach

The pseudo-static approach is widely used to compute seismic loadings by simply assuming uniform accelerations within soil masses in which constant inertial forces are employed to model seismic excitations. However, it fails to characterize the dynamic nature of earthquake motions, for instance, the phase shift because of the finite shear wave propagation [20]. In order to rectify this drawback, the pseudo-dynamic approach is adopted to model the seismic response of earthquake in terms of its duration, periodicity and amplification.

Compared with the pseudo-static approach, the pseudo-dynamic approach has the advantages to consider the amplitude and phase changes of seismic vibrations, the impacts of primary wave velocity and shear wave velocity propagating in soils, and the period of ground shakings.

The propagation of seismic waves in soils is related to the shear wave velocity V_s and the primary wave velocity V_p. When a seismic wave propagates towards the ground surface, its vibrating effect is amplified. It is assumed that the horizontal and vertical seismic accelerations linearly increase from input seismic accelerations (namely $k_h g$ and $k_v g$) at the slope base to amplified values ($f_a k_h g$ and $f_a k_v g$) at the ground surface, where k_h and k_v represent horizontal and vertical seismic coefficients, g is the gravity acceleration, f_a is a soil amplification factor, as sketched in Figure 2(b).

Besides, sinusoidal vibrations are employed to simulate earthquake waves, and there is a phase shift between the slope base and the ground surface (see Figure 2(a)) [19−22]. Thus, in the pseudo-dynamic approach, the horizontal seismic acceleration a_h and the vertical seismic acceleration a_v can be obtained by the following sinusoidal functions in terms of depth z and time t,

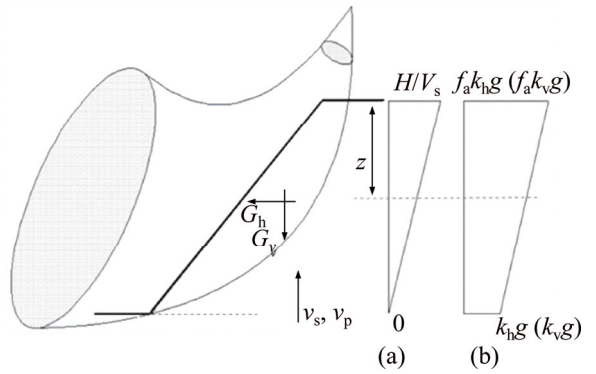

Figure 2 Slopes under pseudo-dynamic loadings in longitudinal symmetry plane: (a) Phase shift; (b) Seismic accelerations change between base and ground surface

$$\begin{cases} a_{\mathrm{h}}(z,t)=\left[1+\dfrac{H-z}{H}(f_{\mathrm{a}}-1)\right]\cdot k_{\mathrm{h}}g\cdot\sin\left(2\pi\left(\dfrac{t}{T}-\dfrac{H-z}{TV_{\mathrm{s}}}\right)\right) \\ a_{\mathrm{v}}(z,t)=\left[1+\dfrac{H-z}{H}(f_{\mathrm{a}}-1)\right]\cdot k_{\mathrm{v}}g\cdot\sin\left(2\pi\left(\dfrac{t}{T}-\dfrac{H-z}{TV_{\mathrm{p}}}\right)\right) \end{cases} \tag{1}$$

where T is the seismic shaking period.

2.3 Work rate calculations

In the kinematical approach of limit analysis, an upper-bound solution can be derived using a work balance equation regarding the external work rates and the internal energy dissipations. In this study, the external forces applied to the slope sliding body are the gravity and inertial forces induced by seismic excitations, and the energy dissipations occur within the volume and along the failure surface. Since the mechanism has been discretized, the total external work rate and the energy dissipations can be obtained by simple summation of those on each discrete element.

As seen in Figure 1, the triangular facet $F_{i,j}$, formed by three points $P_{i,j}$, $P_{i,j+1}$ and $P_{i+1,j+1}$, is an element at the boundary of the failure mechanism; $P'_{i,j}$, $P'_{i,j+1}$, $P'_{i+1,j+1}$ are the projections at the symmetry plane. The entity, corresponding to $F_{i,j}$ and defined by points $P_{i,j}$, $P_{i,j+1}$, $P_{i+1,j+1}$ and their projections at the symmetry plane, is used for computing the work rate of gravity. Work rate of the weight of the block:

$$\dot{W}_{\gamma}=\omega\gamma\sum_{i}\sum_{j}(R_{i,j}V_{i,j}\cos\theta_{i,j}) \tag{2}$$

where $\theta_{i,j}$ and $R_{i,j}$ are the polar coordinates of the barycenter in the triangular facets $F_{i,j}$; $V_{i,j}$ represents the volume of the element of facets $F_{i,j}$; γ is the soil unit weight.

The work rate of horizontal seismic forces:

$$\dot{W}_{\mathrm{kh}}=\omega\gamma\sum_{i}\sum_{j}\left\{[1+\frac{H-z}{H}(f-1)]\cdot k_{\mathrm{h}}\sin\left(2\pi\left(\frac{t}{T}-\frac{H-z}{TV_{\mathrm{s}}}\right)\right)V_{i,j}R_{i,j}\sin\theta_{i,j}\right\} \tag{3}$$

The work rate of vertical seismic forces:

$$\dot{W}_{\mathrm{kv}}=\omega\gamma\sum_{i}\sum_{j}\left\{[1+\frac{H-z}{H}(f-1)]\cdot k_{\mathrm{v}}\sin\left(2\pi\left(\frac{t}{T}-\frac{H-z}{TV_{\mathrm{p}}}\right)\right)V_{i,j}R_{i,j}\cos\theta_{i,j}\right\} \tag{4}$$

The total energy dissipation within volume and over the failure surfaces can be formulated by [7]:

$$\begin{aligned}\dot{W}_{\mathrm{D}}&=c\cot\varphi\int\!\!\int_{s}\vec{v}\cdot\vec{n}\mathrm{d}S\\&=-\omega c\cot\varphi\left[\sum_{i}R_iS_i\cos\theta_i+\sum_{j}R_jS_j\cos(\theta_j+\beta)\right]\end{aligned} \tag{5}$$

where c is the soil cohesion and φ the soil friction angle; S_i and S_j respectively correspond to the area of element at the top surface and the slope surface; θ_i and R_i, (respectively θ_j and R_j) are the polar coordinates of the center of the element at the top surface (respectively the slope surface).

By equating the total external work rate to the total energy dissipation, $\dot{W}_{\gamma}+\dot{W}_{\mathrm{kh}}+\dot{W}_{\mathrm{kv}}=\dot{W}_{\mathrm{D}}$, an upper-bound estimate of slope heights or yield seismic coefficients or safety factors can be derived, which are depended on four parameters that determine the geometry of the failure mechanism, θ_0, θ_{h}, r'_0/r_0, b/H, and the time t. The critical slope heights or critical yield seismic coefficients can be obtained by optimization with respect to these five variables under the constraints: $0<\theta_0<180°$, $\theta_0<\theta_{\mathrm{h}}<180°$, $0<r'_0/r_0<1.0$, $0<B'/H\leq B/H$ and $0<t<T$.

In order to find the global minimum, a hybrid scheme that combines the genetic algorithm and a fast local optimization solver (fminsearch function) is adopted. The genetic algorithm is firstly used to locate the region near an optimum point, followed by a fast local optimization solver (fminsearch function) using the solution from the genetic algorithm as an initial point. The genetic algorithm can reach the region near an optimal point relatively fast, but it converges slowly. On the contrary, the local optimization algorithm, such as “fminsearch

function", is more efficient. Such a hybrid scheme makes a good compromise between accuracy and efficiency.

In this study, the safety factors are computed to evaluate slope stability. In geotechnical engineering, there are two ways of safety factor assessments; one is based on strength reduction (SRM) method by which safety factor is defined as the ratio of the real material strength to the critical strength at the limit equilibrium state and the other is the ratio of material resistance capacity to externally destructive effect. PAN et al [27] show that the SRM is more conservative compared with the resistance-over-loading method and should be used in practical engineering. For Mohr-Coulomb material whose shear strength parameters refer to cohesions and friction angles, the SRM-defined safety factor reads,

$$FS=\frac{c}{c_{FS}}=\frac{\tan\varphi}{\tan\varphi_{FS}} \tag{6}$$

It is of practical interest to note that the proposed deterministic model is very efficient in assessing safety factors of a 3D slope. For example, it costs no more than one minute for one safety factor calculation on an Intel i5-7500 CPU @ 3.4 GHz PC. Such a benefit is helpful for probabilistic analysis since it involves a large number of computing safety factors. Due to this efficient feature, the method of Monte Carlo Simulation can be directly used in this work for probabilistic analysis.

3 MCS-based probabilistic analysis

The reliable assessment of safety factors of a slope using the above presented deterministic model is highly dependent on if the input parameters required are exactly given. However, limited access to geological and geotechnical datum makes it impossible to collect complete information of input parameters in site. This means that uncertainties in input parameters, regarding to soil material properties, structure dimensions and external loadings, always exist, which definitely affect geotechnical structure safety. Probabilistic analysis is commonly adopted to quantify the uncertainties of input parameters by computing failure probabilities of structure responses. Specifically, input parameters are treated as random variables following prescribed distributions, thus the corresponding model response (slope safety factor in this case) is also a random variable.

Monte Carlo Simulation (MCS), the most straightforward and robust approach of assessing failure probabilities, is adopted in this work to assess the failure probability. It proceeds in three steps: 1) randomly sampling a large number of input parameters with underlying PDFs, 2) repeatedly running the limit state function for all sets and 3) computing failure probability using the following equation,

$$\hat{P}_{\mathrm{f}}=\frac{1}{N_{\mathrm{mc}}}\sum_{i=1}^{N_{\mathrm{mc}}}I(G(x)) \tag{7}$$

where N_{mc} is the number of MCS samples; $G(\boldsymbol{x})$ is the limit state function, $I(G)=1$ when $G<0$; otherwise $I(G)=0$. The coefficient of variation (COV) of estimated failure probability is expressed as,

$$COV_{\hat{P}_{\mathrm{f}}}=\sqrt{\frac{1-\hat{P}_{\mathrm{f}}}{N_{\mathrm{mc}}\hat{P}_{\mathrm{f}}}} \tag{8}$$

In this work, the number of MCS N_{mc} is set to be large enough so that $COV_{\hat{P}_{\mathrm{f}}}$ is not bigger than 10%. In this study, the limit state function in terms of safety factor FS of a 3D slope is expressed as,

$$G(\boldsymbol{x})=FS-1 \tag{9}$$

where FS is determined by Eq. (6).

Six pseudo-dynamic input parameters and two soil shear strength parameters are considered as random variables. Their statistical properties are provided in Table 1, making reference to previously published articles [19−22, 28, 29]. The random input variables are assumed to follow lognormal distributions. Other input parameters, the slope angle β, the slope height H, the ratio of slope width to slope height B/H, and soil unit weight γ, are considered as deterministic since they can be easily measured. In the subsequent calculations, the discretization parameters $\delta\theta$ and $\delta\alpha$ are respectively taken to be 0.5° and 1.0° for generating the 3D failure mechanism.

4 Results and discussion

4.1 Influence of horizontal seismic coefficient on computed failure probabilities

Figure 3 presents the impact of the horizontal

Table 1 Configurations of input variables

Parameter	Input variable	Mean	*COV*/%
Pseudo-dynamic parameter	T/m	0.3	10
	f_a	1.2	15
	k_h	0.2	25
	k_v	0.1	25
	V_s/(m·s^{-1})	150	10
	V_p/(m·s^{-1})	280.5	10
Soil material	c/kPa	20	20
	φ/(°)	25	10
	γ/(kN·m^{-3})	20	0
Slope geometry	β/(°)	60	0
	B/H	5	0
	H/m	10	0

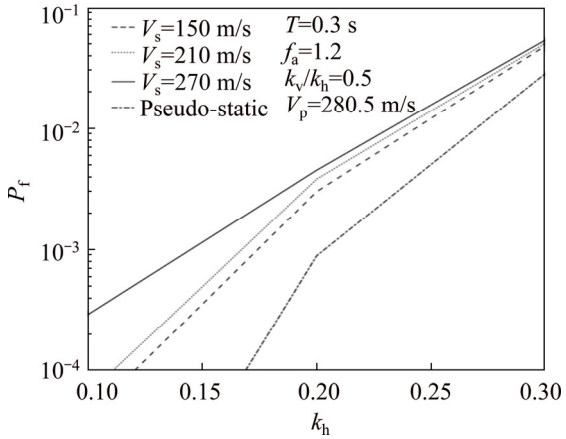

Figure 3 Influence of k_h on failure probabilities under different V_s

seismic coefficients on the obtained failure probabilities. In the calculations, three cases of the mean values of shear velocities are taken into account, changing from 150 to 270 m/s; the mean values of horizontal seismic coefficients range between 0.1 and 0.3. It is observed that the mean values of horizontal seismic coefficients significantly affect the slope failure probabilities. For V_s=270 m/s, the failure probability rises from 1.9×10^{-3} at k_h=0.1 to 5.3×10^{-2} at k_h=0.3, increasing by approximately 2639.5%. The results of the pseudo-static analysis are also provided for analysis. It is seen that the pseudo-static approach gives the smallest failure probabilities compared with the pseudo-dynamic approach. This means that the pseudo-static approach is less conservative than the pseudo-dynamic approach.

4.2 Influence of vertical seismic coefficient on computed failure probabilities

Figure 4 shows the failure probability as a function of the vertical seismic coefficient k_v normalized by its horizontal counterpart k_h. Three mean values of shear velocities are taken into account, and the ratio of k_v/k_h is in the range between 0.2 and 1.0. For example, when the ratio of k_v/k_h changes from 0.2 to 1.0, the failure probability increases from 2.2×10^{-3} to 5.7×10^{-3} for the case of shear wave velocity V_s equal to 150 m/s. The relative increment is about 164.2%.

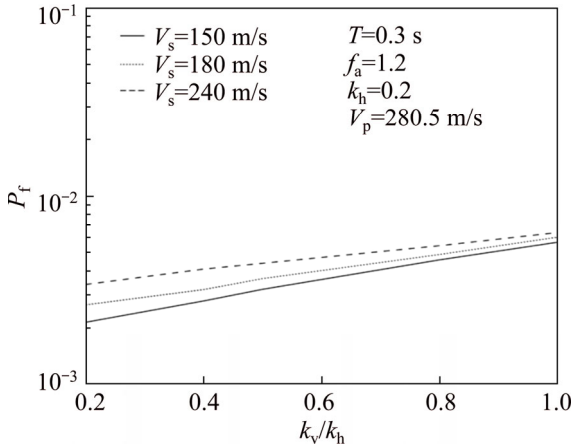

Figure 4 Influence of k_v on failure probabilities under different V_s

4.3 Influence of shear wave velocity on computed failure probabilities

Figure 5 shows the effects of the shear wave velocity V_s on the computed failure probabilities. In the computations, the mean values of shear wave velocity V_s are changed from 160 to 260 m/s, and three mean values of horizontal seismic coefficients, respectively 0.2, 0.3 and 0.4, are adopted. It is seen that the computed failure probabilities slightly increase with the shear wave velocity. For the case of the mean value of k_h being 0.2, the failure probability increases about by 53.3% from 3.0×10^{-3} at V_s=160 m/s to 4.6×10^{-3} at V_s=260 m/s. For the case of the mean value of k_h equal to 0.4, the failure probability increases about by 25.0% from 1.9×10^{-1} at V_s=160 m/s to 2.5×10^{-1} at V_s=260 m/s. This indicates that the influence of shear wave velocity on the computed failure probabilities decreases with the increase of the seismic coefficients. Such a phenomenon can also be observed in Figures 3 and 4.

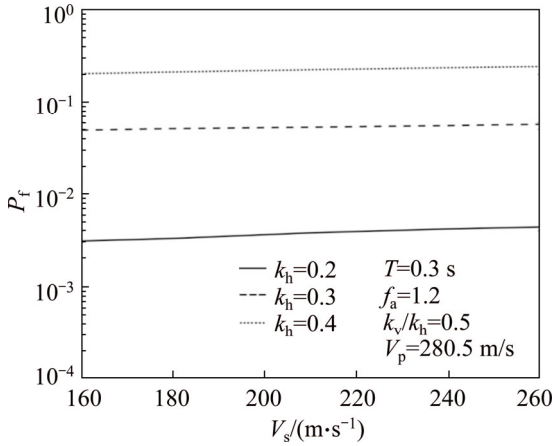

Figure 5 Influence of V_s on failure probabilities under different k_h

4.4 Influence of primary wave velocity on computed failure probabilities

Figure 6 provides the computed failure probabilities as a function of the primary wave velocity V_p ranging from 250 to 400 m/s. In the computations, three mean values of horizontal seismic coefficients are considered. Not surprisingly, what is observed in this plot is similar to that in Figure5; the computed failure probabilities increase with the primary wave velocity.

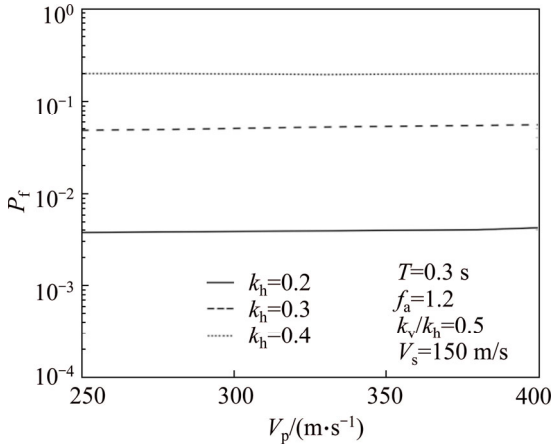

Figure 6 Influence of V_p on failure probabilities under different k_h

4.5 Influence of seismic shaking period on computed failure probabilities

Figure 7 plots the influences of the seismic shaking period T on the computed failure probabilities. In the implemented calculations, the mean values of the seismic shaking period T are set to changes from 0.2 s to 1.0 s, and three mean values of horizontal seismic coefficients adopted are, respectively, 0.2, 0.3 and 0.4. It is observed that the computed failure probabilities are greatly affected by the seismic shaking period. For the case of the mean values of k_h=0.2, the failure probability rises from 2.3×10^{-3} at T=0.2 s to 5.8×10^{-3} at T= 1.0 s, increasing by approximately 152.2%. This is reasonable since the longer the seismic shaking lasts, the higher the failure risk the slope takes.

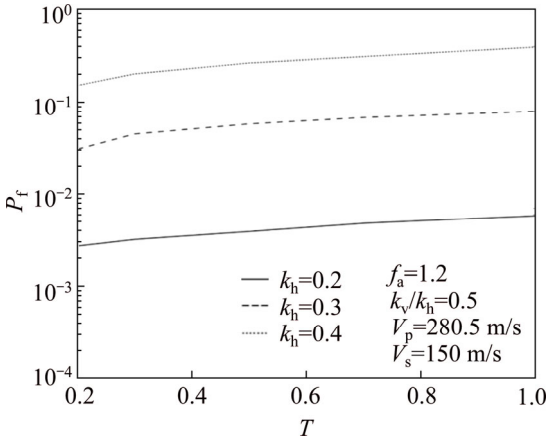

Figure 7 Influence of T on failure probabilities under different k_h

4.6 Influence of soil amplification factor on computed failure probabilities

Figure 8 shows the influence of soil amplification factor f_a on obtained failure probability. In the plot, the mean values of soil amplification factor f_a are varied from 1.0 to 1.8, and three mean values of horizontal seismic coefficients adopted are considered. It is observed that the change of the mean values of the soil amplification factor f_a largely impacts the computed failure probabilities. An increase of the mean values of f_a from 1.0 to 1.8 leads to an increase of the computed failure probabilities from 2.2×10^{-3} to

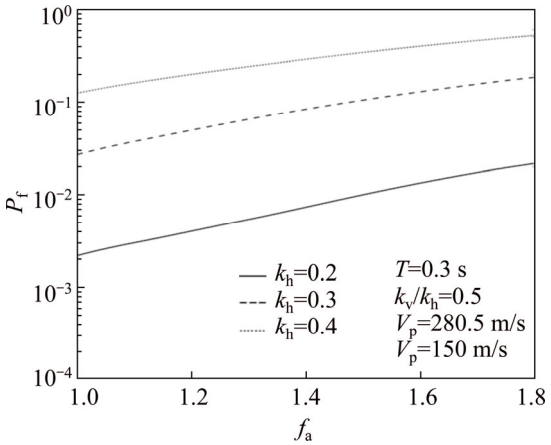

Figure 8 Influence of f_a on failure probabilities under different k_h

2.2×10^{-2} for the case of the horizontal seismic coefficient being 0.2. This phenomenon can be explained well by the fact that the seismic accelerations are proportional to the soil amplification factor as seen in Eq. (1).

5 Conclusions

Probabilistic assessment of seismic slope stability is an important issue in geotechnical engineering, but the complex nature of the problem makes it difficult to implement finite element analyses, which are often associated with high computational demands. Meanwhile, simple pseudo-static approaches may not characterize the dynamic nature of the earthquake ground shakings. In this paper, the pseudo-dynamic approach is adopted to represent seismic loadings, and the slope safety factor is assessed using the kinematical approach of limit analysis. Such a combination leads to an efficient deterministic model to assess safety factors of 3D slopes. Then the method of Monte Carlo Simulation is applied to perform probabilistic analysis in terms of the failure probabilities. Eight random input variables are taken into account, including six pseudo-dynamic input parameters (k_h, k_v, V_s, V_p, T, f_a), two soil shear strength parameters (c, φ).

The influences of six pseudo-dynamic input parameters on computed failure probabilities are discussed. It is shown that the computed failure probabilities increase with the magnitude of all pseudo-dynamic input parameters, especially the horizontal and vertical seismic coefficients and the soil amplification factor. A comparison with the pseudo-static approach indicates that the pseudo-dynamic approach is able to provide more conservative results of failure probabilities. Thus, it is recommended to use the pseudo-dynamic approach in a practical slope design on the safe side.

References

[1] LAM L, FREDLUND D G. A general limit equilibrium model for three-dimensional slope stability analysis [J]. Canadian Geotechnical Journal, 1993, 30(6): 905−919.

[2] XU J S, YANG X L. Seismic stability of 3D soil slope reinforced by geosynthetic with nonlinear failure criterion [J]. Soil Dynamics and Earthquake Engineering, 2019, 118: 86−97.

[3] CHENG Y M, LANSIVAARA T, WEI W B. Two-dimensional slope stability analysis by limit equilibrium and strength reduction methods [J]. Computers and Geotechnics, 2007, 34(3): 137−150.

[4] GRIFFITHS D V, LANE P A. Slope stability analysis by finite elements [J]. Geotechnique, 1999, 49(3): 387−403.

[5] QIN C B, CHIAN S C. Kinematic analysis of seismic slope stability with a discretisation technique and pseudo-dynamic approach: a new perspective [J]. Geotechnique, 2018, 68(6): 492−503.

[6] MICHALOWSKI R L, DRESCHER A. Three-dimensional stability of slopes and excavations [J]. Geotechnique, 2009, 59(10): 839−850.

[7] ZOU J F, QIAN Z H, XIANG X H, CHEN G H. Face stability of a tunnel excavated in saturated nonhomogeneous soils [J]. Tunnelling and Underground Space Technology, 2019, 83(1): 1−17.

[8] GAO Y, ZHU D, ZHANG F, LEI G H, QIN H. Stability analysis of three-dimensional slopes under water drawdown conditions [J]. Canadian Geotechnical Journal, 2014, 51(11): 1355−1364.

[9] QIN C B, CHIAN S C. Seismic stability of geosynthetic-reinforced walls with variable excitation and soil properties: A discretization-based kinematic analysis [J]. Computers and Geotechnics, 2018, 102: 196−205.

[10] ZHANG D B, JIANG Y, YANG X L. Estimation of 3D active earth pressure under nonlinear strength condition [J]. Geomechanics and Engineering, 2019, 17(6): 515−525.

[11] LI Z W, YANG X L. Kinematical analysis of active earth pressure considering tension crack, pore-water pressure and soil nonlinearity [J]. KSCE Journal of Civil Engineering, 2019, 23(1): 56−62.

[12] LI T Z, YANG X L. 3D rotational failure mechanism of tunnel face in weathered and saturated Hoek-Brown rock masses [J]. KSCE Journal of Civil Engineering, 2019, 23(6): 2723−2732.

[13] ZHANG J H, WANG W J, ZHANG B, ZHANG D B. Upper bound analysis for collapse failure of shield tunnel face excavated in unsaturated soils considering steady vertical flow [J]. Mathematical Problems in Engineering, 2019: 214561.

[14] ZHANG R, YANG X L. New 3D failure analysis of water-filled karst cave beneath deep tunnel [J]. Geomechanics and Engineering, 2019, 18(1): 1−9.

[15] ZHANG D B, JIANG Y, YANG X L. Estimation of 3D active earth pressure under nonlinear strength condition [J]. Geomechanics and Engineering, 2019, 17(6): 515−525.

[16] YANG X L, ZHANG S. Seismic active earth pressure for soils with tension cracks [J]. International Journal of Geomechanics, 2019, 19(6): 06019009.

[17] MICHALOWSKI R L, MARTEL T. Stability charts for 3D failures of steep slopes subjected to seismic excitation [J]. Journal of Geotechnical and Geoenvironmental Engineering, 2011, 137(2): 183−189.

[18] PAN Q, DIAS D. Probabilistic stability analysis of a three dimensional rock slope characterized by the Hoek-Brown failure criterion [J]. Journal of Computing in Civil Engineering, 2017, 31(5): 04017046.

[19] STEEDMAN R S, ZENG X. The influence of phase on the

calculation of pseudo-static earth pressure on a retaining wall [J]. Geotechnique, 1990, 40(1): 103−112.
[20] CHOUDHURY D, NIMBALKAR S. Seismic rotational displacement of gravity walls by pseudo-dynamic method: Passive case [J]. Soil Dynamics and Earthquake Engineering, 2007, 27(3): 242−249.
[21] BASHA B M, BABU G S. Reliability assessment of internal stability of reinforced soil structures: A pseudo-dynamic approach [J]. Soil Dynamics and Earthquake Engineering, 2010, 30(5): 336−353.
[22] ESKANDARINEJAD A, SHAFIEE A H. Pseudo-dynamic analysis of seismic stability of reinforced slopes considering non-associated flow rule [J]. Journal of Central South University of Technology, 2011, 18(6): 2091−2099.
[23] LIU L, CHENG Y, WANG X. Genetic algorithm optimized Taylor Kriging surrogate model for system reliability analysis of soil slopes [J]. Landslides, 2017, 14(2): 535−546.
[24] ZHANG J H, WANG W J, ZHANG D B, ZHANG B, MENG F. Safe range of retaining pressure for three-dimensional face of pressurized tunnels based on limit analysis and reliability method [J]. KSCE Journal of Civil Engineering, 2018, 22(11): 4645−4656.
[25] ZHANG W G, GOH A T C. Multivariate adaptive regression splines for analysis of geotechnical engineering systems [J]. Computers and Geotechnics, 2013, 48: 82−95.
[26] YANG X L, ZHANG S. Risk assessment model of tunnel water inrush based on improved attribute mathematical theory [J]. Journal of Central South University, 2018, 25(2): 379−391.
[27] PAN Q, DIAS D. Upper-bound analysis on the face stability of a non-circular tunnel [J]. Tunneling and Underground Space Technology, 2017, 62: 96−102.
[28] ORESTE P. A probabilistic design approach for tunnel supports [J]. Computers and Geotechnics, 2005, 32(7): 520−534.
[29] PHOON K K, KULHAWY F H. Characterization of geotechnical variability [J]. Canadian Geotechnical Journal, 1999, 36(4): 612−624.

(Edited by HE Yun-bin)

中文导读

基于拟动力法的三维边坡稳定性概率分析

摘要：从概率分析的角度进行工程设计是一种合理的方法，它可以提供比传统的确定性分析更全面的信息。本文从概率分析的角度研究了三维边坡地震稳定性。通过结合基于三维旋转破坏机制的极限分析上限法与拟动力法来计算边坡的安全系数。采用蒙特卡罗模拟方法来考虑模型参数的变异性，包括六个拟动力法参数和两个土体抗剪强度参数。本文研究并讨论了拟动力法参数的变异性对计算失效概率的影响。结果表明：边坡的失效概率随着拟动力法参数的增加而增加，与拟静力法相比，拟动力法可以给出更为保守的失效概率估计结果。

关键词：边坡地震稳定性；拟动力法；概率分析；蒙特卡洛模拟；破坏概率；三维边坡